EPJ Web of Conferences **29**, 00009 (2012)
DOI: 10.1051/epjconf/20122900009

Structural characterization of $PbTi0_3$, $Sm_{0.6}Nd_{0.4}NiO_3$ and $NdMnO_3$ multifunctional Perovskite thin films

M. Boudard [a1], C. Girardot[1,2], N. Ihzaz[1,3], S. Pignard[1], L. Rapenne[1], H. Roussel[1], A. Bartasyte[1,4]

[1]Laboratoire des Matériaux et du Génie Physique (CNRS UMR 5628), Minatec Bâtiment INPG, parvis Louis Néel, BP 257, 38016 Grenoble Cedex 1, France
[2]Schneider Electric Industries S.A.S., 37 Quai Paul Louis Merlin, 38050 Grenoble Cedex 9, France
[3]Laboratoire de Physico–Chimie des Matériaux, Faculté des Sciences de Monastir, Département de Physique, 5019, Monastir, Tunisie.
[4]P2M, Institut Jean Lamour, Nancy Université, Bd. des Aiguillettes, 54506 Vandoeuvre-ls-Nancy cedex, France

Abstract. Different multifunctional ($PbTiO_3$, $Sm_{0.6}Nd_{0.4}NiO_3$, $NdMnO_3$) thin films were grown by metalorganic chemical vapor deposition (MOCVD) technique on $SrTiO_3$ and $LaAlO_3$ substrates. TEM and X-ray diffraction measurements reveal that almost single crystalline thin films can be epitaxially grown on the top of substrates. The relationship between the crystallographic orientation of the films and those of the substrates were determined by reciprocal space mapping and TEM analyses. $PbTi0_3$ thin films appear to be under tensile or compressive strain according to the different mismatch of their cell parameter with those of the substrate. Relaxation mechanism as a function of the film thickness arises from coexistence of different type of domains and size and strain effect are analyzed. $SmNiO_3$ thin films present diffuse scattering strikes and are less well organized when compared to $PbTi0_3$ thin films. Different domains are observed as well as an additional parasitic phase close to NiO. Its regular distribution can be associated to reduced transport properties. Preliminary observations on $NdMnO_3$ thin films show that an amorphous phase is obtained during MOCVD that can be transformed in a single crystalline film by annealing. The films are under tensile or compressive strain according to the different mismatch of their cell parameter with those of the substrate. Magnetic properties are investigated.
Keywords: MOCVD, Thin film, Perovskites, X-ray diffraction, TEM.
PACS: 61, 73, 75

1 Introduction

Perovskites oxides are widely used in electronic devices due to their interesting physical properties as by example dielectric (e.g. high K and ferroelectric materials) or magnetic and electrical properties (e.g. magnetoresistive materials)[1, 2]. A rapid and costless research on these materials can be realized through simple synthesis techniques as metalorganic chemical vapor

[a] e-mail : mboudard@minatec.inpg.fr

deposition (MOCVD) [3, 4]. These techniques allow a rapid formatting of perovskite materials in the form of thin film on different substrate and subsequently several important parameters can be studied: phase stability, structural quality, misfit induced effect, etc. In this study we present structural characterization on thin films of $PbTiO_3$, $Sm_{0.6}Nd_{0.4}NiO_3$ and $NdMnO_3$.

2 Experimental

Film depositions were carried out by pulsed injection MOCVD. A few micro liters droplets of an organic solution containing a dissolved mixture of metal-organic precursors are injected and subsequently evaporated and transported by an Ar + O2 gas flow towards the heated substrate where the precursors are adsorbed, diffused and decomposed on its surface. At the end of the deposition a short in situ annealing at 680°C for 30 minutes in a pure oxygen flow is eventually performed. Typical deposition conditions and detailed precursors solutions can be found in [5, 6, 7, 8, 9]. Morphology of the film surface was examined by scanning electron microscopy and atomic force microscopy and composition was checked by energy dispersive X-ray spectroscopy analysis (EDX). Phase purity and crystallization were studied by X-ray diffraction (XRD) in Bragg-Brentano geometry using a BRUKER D8 advance diffractometer with monochromatic Cu $K_{\alpha 1}$ radiation λ = 0.154060 nm and LynxEye 1 dimension detector. Texture and in-plane orientation of the films were studied by XRD in Schulz geometry using a SIEMENS D5000 diffractometer with Cu $K_{\alpha 1}$ and $K_{\alpha 2}$ radiation λ =0.154184 nm and punctual scintillator detector. Microstrain in the films and grain size were estimated from peak broadening of the 00l reflections in $\theta/2\theta$ scans using the Williamson-Hall analysis available in Winplotr [10]. Reciprocal space mapping was performed using a Nonius Kappa CCD diffractometer (see details in [11]). Transmission electron microscopy (TEM) observations were carried out at 200 kV with a JEOL 2010 microscope (0.19 nm resolution). Cross-section samples were prepared by the tripod polishing method [12] using diamond lapping films to achieved sample thickness of about 10 to 20 µm. Low-angle ion beam milling was used for final perforation of the samples to be sure to have a large electron transparent area. Magnetization (M) vs. temperature (T) were measured using both standard extracting sample and squid magnetometers (Quantum Design) with generally applied magnetic field of 0.05 T in field cooled (FC) and zero field cooled (ZFC) regime in 10 − 140 K temperature range.

3 Results and discussion

3. 1. $PbTiO_3$ Thin Films

The aim of this study was the understanding of the variations induced by different misfits and different films thicknesses. On the one side the misfit of the substrate directly affects the effective 2-Dim (lateral) clamping of the film on the substrate, modifying the straining and the elastic energy of the film. On the other side twins naturally form on ferroelectric and ferroelastic materials to achieve stress relief.

Indeed at the deposition temperature PT has a cubic structure and is paraelectric. A phase transition to a stable ferroelectric state at low temperature with tetragonal symmetry takes place at around 500 °C. During this transformation the ferroelectric domains can be developed along different directions in the form of twins. In bulk samples the different possibilities of orientation of the twins correspond to the different choices of the polar axis of the tetragonal ferroelectric phase that can be derived from the high temperature cubic phase. In thin films this scenario can be strongly modified due to clamping and straining induced by the substrate that may alter the type of stable ferroelectric domain with respect to that in bulk PT.

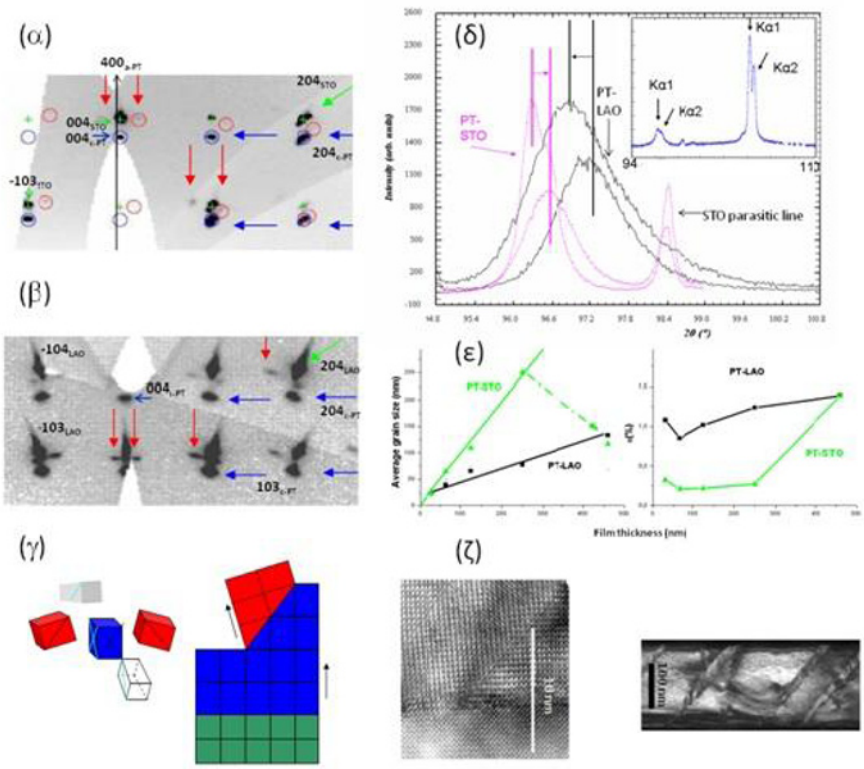

Figure 1. α and β : 2Dim h0l layer obtained from X-ray reciprocal space mapping of a PT film (thickness 460nm) grown on top of STO (α) and LAO (β) substrates. Blue color (circles and arrows) corresponds to c-domains, red color to a-domains and green color (crosses and arrows) to the substrate. γ : Schematic representation of the film on the top of the substrate (green cubes); c-domains (in blue) have an orientation relationship [010]PT //[010]substrate and [100]PT //[100]substrate. The tetragonal axis [001]PT is out of plane in the direction [001]substrate. a-domains in red and gray share a (110) plane with the c-domain. δ : X-ray θ/2θ scan. Qualitative comparison of the widths of the *004* diffraction lines for two PT thin films (thickness 120 and 460 nm) on STO (purple) and on LAO (black). The inset shows $K_{\alpha 1}$ and $K_{\alpha 2}$ splitting for PT film (at low angles) and STO substrate (at high angles on the right side) diffraction lines. ε : Results of Williamson-Hall analysis. Comparison of size effects (left panel) and strain distribution effects (right panel) on the broadening of the diffraction lines as a function of the films thickness for LAO (in black) and STO (in green) substrates. ζ : TEM observations of a- and c-domains for 120 nm thick PT thin film on STO substrate

Along this line thin films of $PbTiO_3$ (hereafter PT) with different thicknesses (30, 60, 120, 250 and 460 nm) were deposited on strontium titanate ($SrTiO_3$ hereafter STO) and lanthanum aluminate ($LaAlO_3$ hereafter LAO). The STO substrate is the best candidate for an epitaxial growth because of its low lattice parameter misfit with that of the PT. The different misfit of the films with the substrates can induce different clamping and straining (with different associated elastic energy) and the different thicknesses can modify the balance of competing interaction arising from clamping and straining on the substrate (dominant for thin films) and from stress relief through twinning (dominant for thick "bulk" films).

Figure 1 represents X-ray and TEM results. α (STO) and β (LAO) show sections through the reciprocal space (k = 0) obtained on the 460 nm thick film. They show the presence of different type of epitaxially grown domains in the films: domains (hereafter noted c-domain) with the c-axis perpendicular to the substrate plane are identified in blue; domains with the a axis roughly perpendicular to the substrate plane and the c-axis is in the plane (hereafter noted a-domains) are identified in red. The colors match with those used in the schematic representation of the film in γ. Figure 1 α (STO) and β (LAO) show the epitaxially grown c-domain on the substrate that results in

diffraction spots aligned along the vertical direction (alignment is almost perfect for STO as can be seen for *204* reflection in α). Substrate and c-domain orientation relationship is [001]PT //[001]substrate and [100]PT //[100]substrate. The additional diffraction spots of lower intensity, correspond to a-domains (see by example red arrow and circles in Fig.1 α and β). This configuration can be explained by twinning along (1,1,0) type planes represented schematically in Fig.1 γ and can be directly observed by electron transmission microscopy as exemplified for 120 nm thick PT film on STO in Fig.1 ζ. The angle of twinning (highly exaggerated in Fig.1 γ) is related to the difference of c and a lattice parameters of the tetragonal PT phase. For films grown on LAO substrate a much larger proportion of a-domains is observed resulting in more intense diffraction spots of a-domains. The diffraction spots of c-domains present a departure from a vertical alignment with diffraction spots of the substrate (see by example reflection *204* in β). A complete Williamson Hall analysis of the angular dependence of the diffraction peak widths (see Fig.1 δ and ε) allows quantifying size and strain effects. Figure 1 δ compares the *004* diffraction lines of the thin films of thickness 120 and 460 nm for STO and LAO substrates. The main points observed are as follows:

1. The full width at half maximum are much larger (two to three times) for films grown on LAO (black) than for those grown on STO (purple) which indicate a lower structural quality in the case of LAO.

2. There is a relaxation across the film for LAO substrate (asymmetric peak) with an increased lattice parameter (displacement to the left indicates by a black arrow) for thicker films. For STO substrate (purple) we observed an opposite evolution (indicated by a purple arrow) corresponding to a decrease of c cell parameter with thickness.

The Fig.1 ε shows that up to 250 nm the PT's film on STO appears as epitaxially grown (green curve) with grain sizes close to the thickness of the films and strain effect are nearly constant and relatively low (the strain are represented on the right part of the Fig.1 ε by the parameter ε which characterizes a distribution of lattice parameter expressed as relative variation of lattice parameter). For the film thickness of 460 nm there is an increase of strain effects accompanied by a decrease in grain size by a factor of two and corresponds to massive development of a-domains in the film as usually observed for bulk samples (ferroelectric domains with different orientation are formed to minimize the energy associated to ferroelectricity and ferroelasticity). All the films grown on LAO substrates had lower structural quality when compared to films grown on STO substrates with much smaller values of grain size and much larger values of strain distribution.

3. 2. Conclusions (PT Films)

For thicknesses of thin films of PT lower or equal to 250 nm, the in plane parameter of the film is very close to the in the plane parameter of the substrate STO. This low misfit results in clamping of the film on the substrate with a very good epitaxy and with almost no strain distribution. The film is mainly composed of a single crystalline c-type domain characterized by a tetragonal axis perpendicular to the substrate. The film with 460 nm thickness had lower structural quality with strongly reduced correlations lengths and an increased strain distribution that are associated with an increased proportion of a-domains resulting from a stress relief mechanism through twins similarly to what is observed for bulk samples.

The films on LAO present similar stress relief mechanism through twins for all the thicknesses due to the large mismatch with the substrate that reduced the clamping effects. Films are qualitatively similar to 460 nm thick film on STO with grain size smaller than the film thickness and large values of strain distribution.

3. 3. $Sm_{0.6}Nd_{0.4}NiO_3$ ThinFilms

The synthesis of rare-earth nickelates $RNiO_3$ needs either high oxygen partial pressure [13, 14] or the use of a substrate which stabilizes the epitaxial growth of the phase. In this case $RNiO_3$ can be only synthesized on cubic or pseudocubic single crystalline substrates presenting a lattice parameter

close to that of the nickelate [15] (the stress imposed by the substrate on the film leads to the stabilization of the nickelate phase).

For $RNiO_3$ thin films the lattice match between film and substrate as well as the sign of the mismatch is known to strongly influence the electronic transport properties namely the insulator to metal (IM) transition which is characteristic of most rare earth nickelates. For example in $SmNiO_3$ (SNO) thin films, the IM transition is obtained with a strong sharpness at the transition temperature TIM=393 K when deposited on LAO whereas a pure insulator behavior is observed when films are grown on STO substrate [16]. X-ray diffraction space mapping and TEM observations have been achieved in order to correlate the electronic transport behavior with the structural characteristics of $Sm_{0.6}Nd_{0.4}NiO_3$ (SNNO) thin films (Fig. 2). Main Bragg reflections with integer h indices of the thin film are clearly seen nearby reflections of the STO substrate (Fig.2 α) whereas they cannot be distinguished from those of the LAO substrate owing to the lower mismatch (Fig.2 β). Bragg reflections with half integer indices are seen along the l direction for both LAO and STO substrates. Additional Bragg reflections correspond to the NiO phase with different orientation relationship with the substrate : $[100]_{NiO}//[100]_{LAO}$ and $[011]_{NiO}//[010]_{LAO}$; $[-10-1]_{NiO}//[100]_{LAO}$ and $[010]_{NiO}//[010]_{LAO}$; $[100]_{NiO}//[100]_{STO}$ and $[010]_{NiO}//[010]_{STO}$.

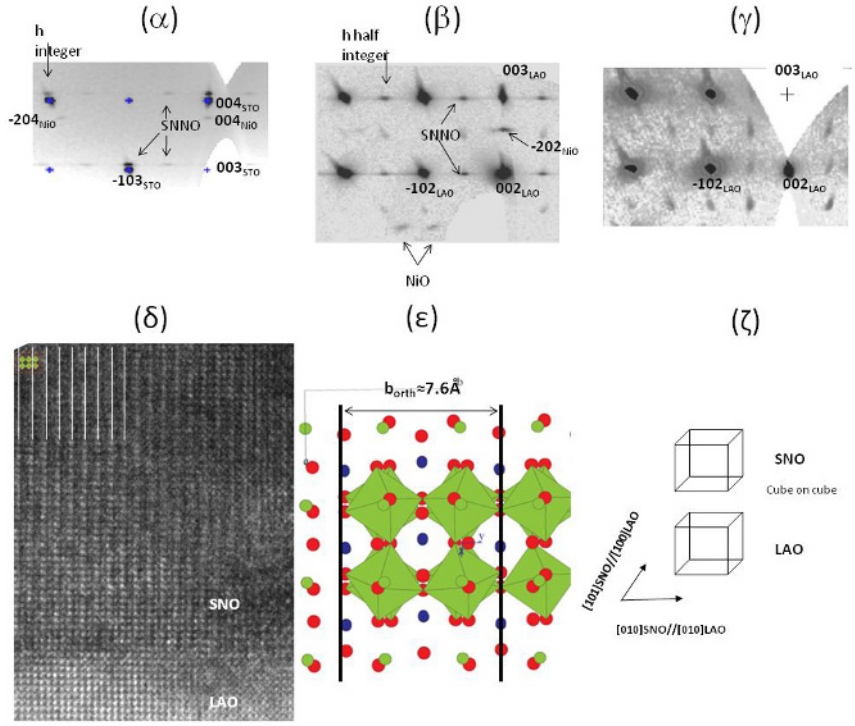

Figure 2. (α to γ): 2Dim h0l layer obtained from X-ray reciprocal space mapping. (α) SNNO film on STO substrate. (β) SNNO film on LAO substrate (γ) LAO substrate alone. (δ) High resolution electron image on SNO film on LAO (ε) and (ζ) are schematic representations of the orientation relationship.

The Fig.2 δ shows a cube on cube orientation relationship of an orthorhombic SNO domain with the LAO substrate. The respective h0l layer of the reciprocal space (not shown) is similar to Fig.2 α and β and similar epitaxy (Fig.2 δ) is expected for SNNO films. A schematic representation of the orientation relationship is given in Fig.2 ε and ζ. Distances between two black lines in Fig.2 ε are equal to b_{orth} SNO cell parameter and correspond to white lines of Fig.2 δ. The long b_{orth} axis of the orthorhombic phase is along the horizontal direction of Fig.2. The orientation relationship is $[010]_{SNO}//[010]_{LAO}$ and $[101]_{SNO}//[100]_{LAO}$; the $[001]_{LAO}$ is the out of plane direction (pseudocubic setting for the LAO substrate and orthorhombic setting for the SNO film).

3. 4. Conclusions (SNNO Films)

Stable SNNO films can be obtained on LAO and STO substrates. Different domains are observed corresponding mainly to domains with $[010]_{SmNiO3}//[010]_{substrate}$ and $[010]_{SmNiO3}//[100]_{substrate}$. A small amount of NiO is observed with different orientation relationship ($[100]_{NiO}//[100]_{LAO}$ and $[011]_{NiO}//[010]_{LAO}$; $[-10-1]_{NiO}//[100]_{LAO}$ and $[010]_{NiO}//[010]_{LAO}$ for LAO substrate). Films deposited on LaO and STO appear to be highly disordered (as can bee seen from diffuse strikes in Fig.2) and high resolution electron images (not shown) indicates that STO films are less well organized. Large region of well crystallized NiO phase could be identified for these films with the orientation relationship $[100]_{NiO}//[100]_{STO}$ and $[010]_{NiO}//[010]_{STO}$. These observations can be related to the different electronic transport properties obtained on LAO and STO substrates.

3. 5. NdMnO3 Thin Films

We report on preliminary results on the growth and characterization of $NdMnO_3$ (hereafter NMO) perovskite thin films grown under epitaxial strain. Our films show an amorphous phase obtained during MOCVD that can be transformed in a single crystalline film by annealing at 900 °C for 24 hours. Highly in-plane oriented thin films, with thickness down to 200 nm (Nd/Mn ratio (EDX)= 0.88) and 150 nm (Nd/Mn ratio (EDX)= 0.96) grown on STO (001) substrate were characterized by X-ray diffraction (see bottom part in Fig.3 α). Bragg reflections *h0h* of the thin films are clearly seen nearby *00l* reflections of the substrate and are much more important for the 150 nm thick film. Furthermore, the sharpness of the diffraction peaks of the NMO 150 nm thick film and the fact that the *h0h* Bragg reflection almost coincide with *00l* Bragg peaks of STO (c_{STO}=0.3905 nm) indicates that this film is epitaxially grown on the substrate with similar orientation relationship that in the previous section [15, 17]. This means that the NMO 150 nm thick film grown on the STO substrate presents a fairly good crystallinity and a strong in-plane texture with the [101]-axis perpendicular to the surface of the substrate. No other peaks are visible, suggesting a single orientation and the absence of second-phase precipitates. The film pseudo-cubic cell parameter, perpendicular to the surface of the substrate, which can be deduced from the scan are 0.3863 nm (Nd/Mn= 0.88) and 0.3859 nm (Nd/Mn= 0.96). According to high resolution electron images of NMO 150 nm thick film (Nd/Mn= 0.96) presented in Fig.3 (β), well-defined orientation relationships at the vicinity of the interface between film and substrate can be identified as: $[010]_{NMO}//[010]_{STO}$ $[101]_{NMO}//[001]_{STO}$. Growth morphology of the MOCVD as grown film can be roughly described as a coexistence of both epitaxial crystalline region near the interface with the substrate and large amorphous regions at the top part of the film. Subsequent annealing at 900 °C for 24 hours improves the quality of the film and results in sharp diffraction peaks as can be seen in the top part of Fig.3 α. Further strong indication of improvement of the film quality are given by magnetic measurements. Indeed Fig.3 γ shows that both blue ZFC and FC curves at 500 Oe are similar whatever the sample is in the form of an annealed film (top part of the figure) or in the form of ceramic powder samples [9, 18] with similar composition (bottom part of the figure).

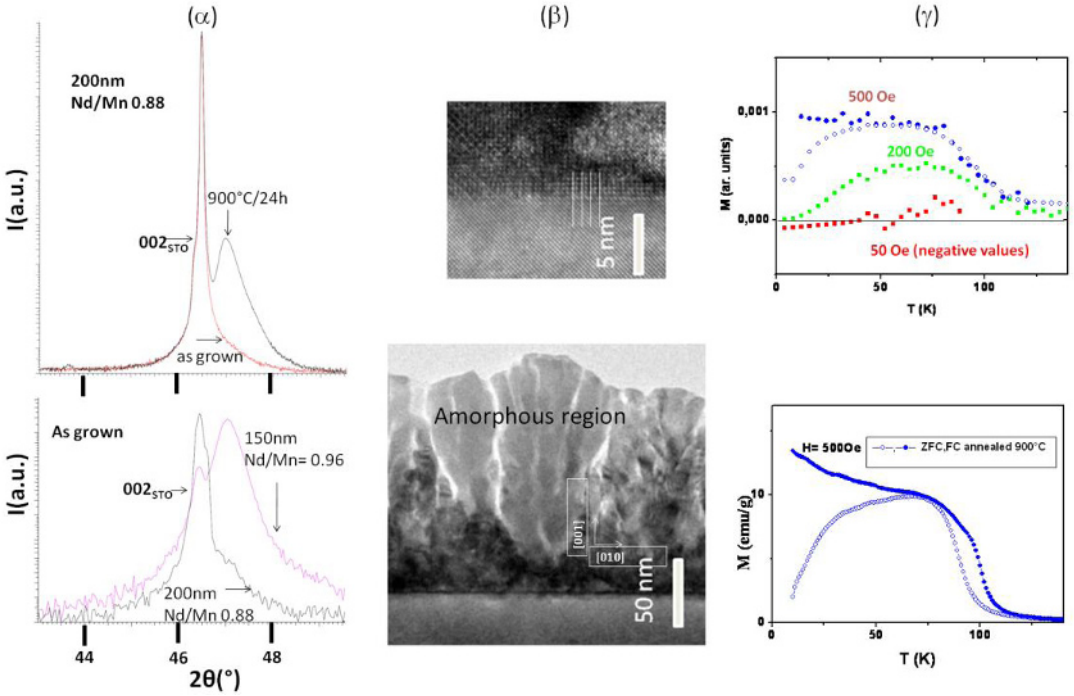

Figure 3. (α) θ/2θ X-ray diffraction pattern of NMO/STO films. Bottom: MOCVD as grown films with two different growing conditions. Top: Improvement of the 200nm thick thin film quality due to annealing. (β) TEM observations on the as grown 150 nm thick film (Nd/Mn ratio of 0.96). Top: Part of the film is epitaxially grown on the STO substrate with $[010]_{NMO}//[010]_{STO}$ and $[101]_{NMO}//[001]_{STO}$. White lines indicate borth cell parameter. Bottom: Large amorphous regions are present on the top part of the film. (γ) Magnetic measurements. Top: Squid magnetometer results on the annealed film at 900 °C for 24 hours (sample thickness 200 nm Nd/Mn ratio (EDX) = 0.88). Bottom: ZFC, FC curves for ceramic powder samples with similar composition.

Acknowledgments

N. Ihzaz, S. Pignard and M. Boudard gratefully thanks financial support from DGRSRT/CNRS (project no 21802).

References

1. A. S. Bhalla, R. Guo, R. Roy, Materials Research Innovations **4**, 3–26 (2000).
2. R. Mitchell, *Perovskites Modern and Ancient*, ISBN 0 9689411 0 9, Almaz press edition, 2002.
3. F. Weiss, U. Schmatz, A. Pisch, F. Felten, S. Pignard, J. P. Sénateur, A. Abrutis, K. Fröhlich, D. Selbmann, L. Klippe, Journal of Alloys and Compounds **251**, 264 – 269 (1997).
4. R. W. Schwartz, Chemistry of Materials **9**, 2325–2340 (1997).
5. C. Girardot, "Structure et propriétés physiques de Films Minces $RENiO_3$ élaborés par MOCVD" Ph.D. Thesis, LMGP-INPG, Grenoble, France, 2009.
6. A. Bartasyte, O. Chaix-Pluchery, J. Kreisel, C. Jimenez, F. Weiss, A. Abrutis, Z. Saltyte, M. Boudard, Journal of Applied Physics **103**, 014103-014110 (2008).
7. A. Bartasyte, O. Chaix-Pluchery, J. Kreisel, J. Santiso, M. Boudard, C. Jimenez, A. Abrutis, F. Weiss, IEEE Transactions on Ultrasonics, Ferroelectrics and Frequency Control **54,** 2623–2631 (2007).

8. A. Bartasyte, "Effet des contraintes et transition de phase dans des couches minces de $PbTiO_3$ obtenus par MOCVD", Ph.D. Thesis, LMGP-INPG, Grenoble, France, 2007
9. N. Ihzaz, "Synthesis, structure and magnetotransport study of Perovskite magnetic oxide", Ph.D. Thesis, INPG/FSM, Grenoble, France, 2008.
10. T. Roisnel, J. Rodriguez-Carvajal, Materials Science Forum **118,** 378 – 381 (2001).
11. P. A. Thomas, S. Trujillo, M. Boudard, S. Gorfman, J. Kreisel, Solid State Science **479**, 1–7 (2009).
12. J. Ayachea, P. H. Albarède, Ultramicroscopy **60,** 195 – 206 (1995).
13. G. Demazeau, A. Marbeuf, M. Pouchard, P. Hagenmuller, Journal of Solid State Chemistry **3**, 582 – 589 (1971).
14. P. Lacorre, J. B. Torrance, J. Pannetier, A. I. Nazzal, P. W. Wang, T. C. Huang, Journal of Solid State Chemistry **91,** 225 – 237 (1991).
15. C. Girardot, F. Conchon, A. Boulle, P. Chaudouet, N. Caillault, J. Kreisel, R. Guinebretière, F. Weiss, S. Pignard, Surface and Coatings Technology **201** 9021 – 9024 (2007). Euro CVD 16, 16th European Conference on Chemical Vapor Deposition.
16. F. Conchon, A. Boulle, R. Guinebretière, C. Girardot, S. Pignard, J. Kreisel, F. Weiss, E. Dooryhée, J.-L. Hodeau, Applied Physics Letters **91**, 192110 (2007).
17. N. Ihzaz, S. Pignard, J. Kreisel, H. Vincent, J. Marcus, J. Dhahri, M. Oumezzine, physica status solidi (c) **1**, 1679–1682 (2004).
18. N. Ihzaz, M. Boudard, H. Vincent, M. Oumezzine, Journal of Alloys and Compounds **479**, 445–450 (2009).